Dalton Transactions

Accepted Manuscript

This is an *Accepted Manuscript*, which has been through the Royal Society of Chemistry peer review process and has been accepted for publication.

Accepted Manuscripts are published online shortly after acceptance, before technical editing, formatting and proof reading. Using this free service, authors can make their results available to the community, in citable form, before we publish the edited article. We will replace this *Accepted Manuscript* with the edited and formatted *Advance Article* as soon as it is available.

You can find more information about *Accepted Manuscripts* in the Information for Authors.

Please note that technical editing may introduce minor changes to the text and/or graphics, which may alter content. The journal's standard Terms & Conditions and the Ethical guidelines still apply. In no event shall the Royal Society of Chemistry be held responsible for any errors or omissions in this *Accepted Manuscript* or any consequences arising from the use of any information it contains.

ROYAL SOCIETY OF CHEMISTRY

www.rsc.org/dalton

Synthesis of morphology controllable porous Co_3O_4 nanostructures with tunable textural properties and their catalytic application

Mouni Roy, Sourav Ghosh, and Milan Kanti Naskar*

Sol-Gel Division, CSIR-Central Glass and Ceramic Research Institute, Kolkata 700 032, India

Abstract: Porous cobalt oxide (Co_3O_4) nanorod (50-100 nm) and nanosheet-like (70-100 nm) particles were synthesized by a facile hydrothermal method at 150^oC for 2-5h and 12-24h, respectively using aqueous-based precursors like cobalt nitrate, urea and water in the absence of any templating agents followed by their calcination at 300^oC. Morphology and textural properties were tuned by changing the synthesis time at 150^oC. 3D architecture of Co_3O_4 was formed by the self-assembly of nanostructured (nanorod and nanosheet) particles. The BET surface area, pore volume and pore diameter of the sample prepared at 150^oC for 5h were 112 m^2g^{-1}, 0.5 cm^3g^{-1} and 7.4 nm, respectively, and it exhibited the highest catalytic performance with a rate constant of $56.8x10^{-3}$ min^{-1} for the degradation of Chicago Sky Blue 6B, a carcinogenic azo dye used in textile, paper and food industries. Rod-like particles with mesoporous structure rendered better catalytic efficiency than sheet-like particles having both the microporous and mesoporous structures. An interrelationship among morphology, textural properties and catalytic efficiency of Co_3O_4 was established.

*Corresponding author. E-mail: milan@cgcri.res.in, Fax: +91 33 24730957

1. Introduction

Transition metal oxides with varied morphologies have attracted intensive research interest because of their possible applications in materials science and engineering. Morphological tuning of the materials is important because it influences in different

Dalton Transactions Accepted Manuscript

properties of the materials. Among the transition metal oxides, tricobalt tetraoxide (Co_3O_4) finds widespread applications in chemical sensor,[1] lithium-ion batteries,[2] optical and magnetic materials,[3,4] and heterogeneous catalysts,[5] where their properties are strongly dependent on their size and shape.[6] In recent years, Co_3O_4 with various morphologies such as nanorods,[7] nanowires,[8] nanotubes,[9] nanobelts,[10] nanocubes,[11] nanosheets[12,13] etc. have been synthesized successfully.

Porous transition metal oxides are of special research interest in finding potential applications in catalysis, sensors, electrode materials for batteries etc.,[14,15] because of their large internal surface area, nanosized walls, and d electrons in an open shell. Mesoporous Co_3O_4 has been proved to be an excellent catalyst for many applications like CH_4 combustion,[16] oxygen evolution,[17] oxidation of toluene and methanol[18] etc. The higher surface area of mesoporous Co_3O_4 renders catalytically more active with facilitating the adsorption and diffusion of reactant molecules, which favours the catalytic performance of the oxides. It is reported that mesoporous Co_3O_4 is generally synthesized by either hard templating route using KIT-6, SBA-15 and SBA-16 silica,[19,20] and carbon spheres[16] as hard templates or soft templating process[21] using Pluronic block copolymer as soft templating agent. The templating methods are tedious and complicated with extra processing time for the removal of the templates. However, there are few reports for the synthesis of mesoporous Co_3O_4 by template-free method. Li *et al.*[22] synthesized mesoporous quasi-single-crystalline Co_3O_4 nanowire arrays on different substrate, like transparent conductive glass, Si wafer and Cu foil. In a recent time, Venugopal *et al.*[23] have reported the preparation of self-assembled hollow mesoporous Co_3O_4 using Li_2O_2 as oxidizing/precipitating agent. Wang *et al.*[24] have prepared different shaped Co_3O_4 using hydrothermal method. Zheng *et al.*[25] synthesized flower-like mesoporous Co_3O_4 by solvothermal method.

Dalton Transactions Accepted Manuscript

In the present study, we have synthesized porous Co_3O_4 nanostructures of tunable morphology and textural properties via a facile one-pot hydrothermal process at 150^oC by changing the reaction times from 2h-24h in the presence of water-based precursors without using any templating agents followed by calcination at 300^oC. The synthesized particles of different morphologies have been used as catalyst for the degradation of Chicago Sky Blue 6B (CSB), a carcinogenic azo dye used in textile, paper, food and pharmaceutical industries.[26] Herein, to the best of our knowledge, we report for the first time a combined role of morphology, surface area, pore volume and pore geometry of Co_3O_4 particles on their catalytic efficiency, and their interrelationship.

2. Experimental

2.1 Synthesis of Co_3O_4 nanostructures

In a typical preparation, cobalt nitrate hexahydrate, $Co(NO_3)_2.6H_2O$ (5 mmol) and urea, $CO(NH_2)_2$ (25 mmol) were dissolved in 50 mL of deionized (DI) water under stirring. Then the above solution was transferred into a 100 mL Teflon-lined autoclave, followed by a hydrothermal treatment at 150^oC for 2h, 5h, 12h and 24h. After the reaction, the samples were collected by centrifugation and washing with DI water, and dried at 60^oC for 4h. The dried as-prepared samples were calcined at 300^oC with a heating rate of 1$^oCmin^{-1}$ and dwell time of 2h each to obtain Co_3O_4 nanostructures.

2.2 Characterizations

X-ray diffraction (XRD) studies of the calcined powders were performed by Philips X'Pert Pro PW 3050/60 powder diffractometer using Ni-filtered Cu-K_α radiation (λ = 0.15418 nm) operated at 40 kV and 30 mA. The thermal behaviours of the uncalcined (as-prepared) particles were studied by thermogravimetry (TG) and differential thermal analysis (DTA)

Dalton Transactions Accepted Manuscript

with (Netzsch STA 449C, Germany) from room temperature to 600^{o}C in air atmosphere at the heating rate of 10^{o}C/min. The characteristic vibration bands of the products were confirmed by FTIR (Nicolet 5PC, Nicolet Analytical Instruments, Madison, WI) with KBr pellet at a resolution of 4 cm^{-1}. The Raman spectrum was recorded with a RENISHAW spectrometer with 514 nm radiation from an argon laser at room temperature. .Nitrogen adsorption-desorption measurements were conducted at 77 K with a Quantachrome (ASIQ MP) instrument. The samples were outgassed in vacuum at 250^{o}C for 4 h prior to the measurement. The surface area was obtained using Brunauer-Emmet-Teller (BET) method within the relative pressure (P/P_o) range of 0.05-0.20 and the pore size distribution was calculated by Barret-Joyner-Halenda (BJH) method. The nitrogen adsorption volume at the relative pressure (P/P_o) of 0.99 was used to determine the pore volume. The morphology of the particles was examined by field emission scanning electron microscopy, FESEM with Zeiss, Supra^{TM} 35VP instrument operating with an accelerating voltage of 10 kV, and transmission electron microscopy, TEM using a Tecnai G2 30ST (FEI) instrument operating at 300 kV. The UV visible spectra were recorded using UV-visible-NIR spectrophotometer (UV – 3101PC, Shimadzu).

2.3 Catalytic Test

In a typical catalytic test, 10 mg of the sample was mixed with 4 mL of 10^{-4} M Chicago Sky Blue 6B (CSB) dye followed by the addition of 0.44 mL hydrogen peroxide, H_2O_2 (30 %). The final dye (40 mL) concentration was adjusted to 10^{-5} M. The reaction mixture was monitored after a fixed interval of time using UV visible spectrophotometer. The decrease in absorption intensity at λ_{max} = 618 nm was observed. The kinetic equations are:

$$C_t/C_o = A_t/A_o \qquad \text{(i)}$$

$$\ln (C_t/C_o) = -kt \qquad \text{(ii)}$$

Dalton Transactions Accepted Manuscript

where, C_t is the dye concentration at time t, C_o is the initial dye concentration, A_t and A_o are absorption intensity at λ_{max} = 618 nm at time t and 0 respectively, and k is the rate constant of the reaction. The degradation efficiency of the catalyst was calculated as $1\text{-}C_t/C_o$. The structure of Chicago sky blue dye is as

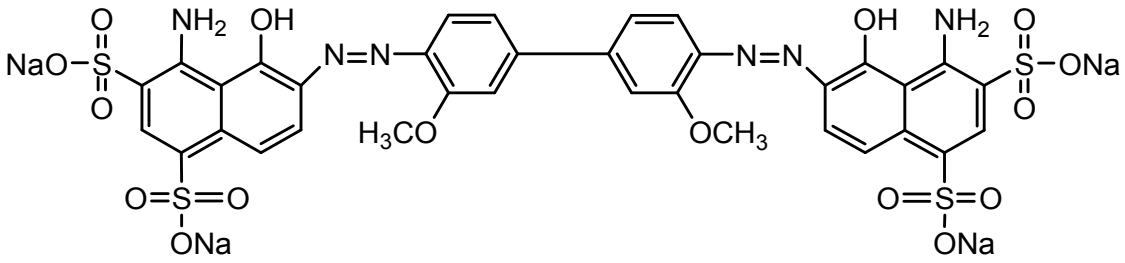

3. Results and discussion

3.1 Characterization of Co_3O_4 nanostructure

Figure 1A shows the XRD patterns of the as-prepared samples indicating the different forms of cobalt hydroxy carbonate. The sample prepared at 150°C for 2h reaction time resulted orthorhombic hydrated cobalt hydroxy carbonate, $Co(OH)_x(CO_3)_{0.5}.\ 0.11H_2O$ (JCPDS File No. 48-0083). Monoclinic cobalt hydroxy carbonate, $Co_2(OH)_2(CO_3)$ (JCPDS File No. 29-1416) phase appeared in the presence of orthorhombic hydrated cobalt hydroxy carbonate phase for 5h reaction time. However, a complete transformation to monoclinic cobalt hydroxy carbonate occurred for 12h and 24h synthesis time at 150°C. After calcination at 300°C, cubic Co_3O_4 phase (JCPDS File No. 43-1003) was formed for all the samples prepared at 150°C for 2h, 5h, 12h and 24h (Fig. 1B). It is to be noted that the presence of Co^{2+} in the raw materials is octahedrally coordinated by lattice oxygen, and it is metastable form. The Co_3O_4 has a spinel structure containing Co^{3+} in an octahedral coordination and Co^{2+} in a tetrahedral coordination,[27] which is thermodynamically stable. Therefore,

Dalton Transactions Accepted Manuscript

calcination of the as-prepared hydrated cobalt hydroxy carbonate and cobalt hydroxy carbonate in air atmosphere, the thermodynamically stable Co_3O_4 spinel was formed.

The DTA and TG analysis of the as-prepared (uncalcined) samples is shown in Fig. S1 (ESI). For 2h reaction time (Fig. S1a), DTA curve shows the endothermic peaks at around 165^{o}C, 260^{o}C and 285^{o}C accompanying with sharp mass loss of 27% up to 300^{o}C in TG curve, while the sample obtained for 5h reaction time shows the endothermic peaks at around 260^{o}C and 290^{o}C with a sharp mass loss of 24.5% up to 300^{o}C (Fig. S1b). Interestingly, for 12h (Fig. S1c) and 24h (Fig. S1d) reaction times, DTA curves exhibit the endothermic peaks at around 290^{o}C and 300^{o}C, respectively. The TG results of 12h and 24h reaction times indicate the sharp mass loss of 22.5% each up to 300^{o}C and 315^{o}C, respectively. The endothermic peaks of all the samples corresponded to the removal of hydroxyl and carbonates. The total mass losses of the samples derived from 2h and 5h reaction times were 29% and 26.5%, respectively while those for 12h and 24h synthesis times, 24% mass loss was obtained. It demonstrated that more decomposable substances were present for 2h and 5h reaction times compared to 12h and 24h times, which corroborated to the XRD results indicating the formation of $Co(OH)_x(CO_3)_{0.5}$. $0.11H_2O$ and $Co_2(OH)_2(CO_3)$ phases, respectively.

The FTIR spectra of the uncalcined and calcined samples are shown in Fig. 2A and 2B, respectively. For the uncalcined samples (Fig. 2A), the absorption band at around 3500 cm^{-1} was assigned to the stretching vibration of O-H group of water, while that appeared at around 3380 cm^{-1} demonstrated the O-H groups interacting with carbonate anions. The absorption bands at around 1550 cm^{-1} and 1410 cm^{-1} was due to the asymmetric stretching vibrations of CO_3^{2-}.[28] The symmetric stretching vibration of CO_3^{2-} ions was noticed at around 1070 cm^{-1}. The presence of nitrate ions in the as-prepared samples was evident from the absorption bands at around 1340 cm^{-1} except for 2h sample which was 1380 cm^{-1}. The

Dalton Transactions Accepted Manuscript

absorption band at 970 cm^{-1} was assigned to M-OH bending mode of vibration. The sharp peak at 830 cm^{-1} corroborated to $\delta(CO_3)$.[29] It is interesting that for the calcined samples (Fig. 2B), two sharp absorption bands were noticed at 565 cm^{-1} and 657 cm^{-1}, which corresponded to spinel Co-O stretching vibration mode;[30] the former peak was assigned to octahedrally co-ordinated Co^{3+}, while the latter was due to tetrahedrally co-ordinated Co^{2+}. Raman spectra of Co_3O_4 prepared at 150^oC for (a) 2h, (b) 5h, (c) 12h and (d) 24h is shown in Fig. 3. The characteristic bands at 195 cm^{-1}, 526 cm^{-1} and 618 cm^{-1} were attributed to the F_{2g} Raman active modes, and those appeared at 484 cm^{-1} and 692 cm^{-1} were due to E_g and A_{1g} modes, respectively. The Raman mode A_{1g} corresponded to the characteristics of octahedral sites, and E_g and F_{2g} modes were assigned to the combined vibrations of tetrahedral site and octahedral oxygen motions.[31]

Figure 4A shows the nitrogen adsorption-desorption isotherms of the calcined (300^oC) samples obtained after hydrothermal synthesis at 150^oC for (a) 2h, (b) 5h, (c) 12h and (d) 24h. It displays type IV isotherm plots according to IUPAC classification, which indicated mesoporous characteristic of the sample. The samples prepared for 2h and 5h shows type H-3 hysteresis loop. It indicated that asymmetric, interconnected, slit-like mesoporosity existed in the samples. However, the samples prepared for 12h and 24h shows type H-4 hysteresis loop. It signified narrow slit-like pores in the structures, and the trend of pore size distribution was toward micropore region. It is to be noted that the samples prepared for 12h and 24h revealed hysteresis loops at relatively lower P/P_o with the appearance of almost horizontal plateau. It also indicated the presence of some microporosity in the samples. The BJH pore size distributions (PSDs) derived from desorption data of the isotherms are shown in Fig. 4B. It reveals wider PSDs in the mesopore region for 2h and 5h-treated samples. However, the samples prepared for 12h and 24h exhibited narrower PSDs nearing micropore region. Table S1 (ESI) summarizes the textural properties of the samples. The BET surface area increased

Dalton Transactions Accepted Manuscript

with increasing reaction times from 2h to 24h. However, the total pore volume increased from 2h to 5h followed by decreasing trend from 5h to 24h. Interestingly, a largest pore size of 10.1 nm was obtained for 2h sample, which decreased on increasing reaction time. It can be explained that at the initial stage of reaction (2h), the nucleation and growth of the particles just started. As a result, larger interparticle spacing among hydrated cobalt hydroxy carbonate ($Co(OH)_x(CO_3)_{0.5}.\ 0.11H_2O$) particles rendered larger pore size of Co_3O_4 upon calcination. With increasing reaction times (12h and 24h), a maximum nucleation and growth of cobalt hydroxy carbonate ($Co_2(OH)_2(CO_3)$) particles minimized the interparticle spacing, and thus, lowered the pore size of the calcined product (Co_3O_4). For 5h-treated sample, the intermediate nucleation and growth in the presence of $Co(OH)_x(CO_3)_{0.5}.\ 0.11H_2O$ and $Co_2(OH)_2(CO_3)$ rendered the pore size of 7.4 nm. The complete nucleation and growth of the particles favoured closure interparticle distance resulting smaller pore size. It is mentioned worthy that there is a decrease trend in pore volumes for the samples obtained from 5h to 24h reaction times. The presence of microporosity for 12h and 24h prepared samples (Table S1) could be the reason for lowering the pore volume. With increasing reaction time, the growth of the particles increased rendering partly closure of relatively large pores (mesopores) and favouring the generation of many smaller pores (micropores). Thus, the plenty of micropores in the samples resulted with higher BET surface area than mere presence of mesopores.

Figure 5 shows the FESEM microstructures of the as-prepared samples obtained hydrothermally at 150^{o}C for (a) 2h, (b) 5h, (c) 12h and (d) 24h. It is clear that chrysanthemum-like morphology of cobalt hydroxy carbonate was obtained for 2h and 5h hydrothermal reaction times. The diameter of the particles was ~5 μm, consisting of a number of self-assembled nanorods of diameter 50-100nm. However, with increase in reaction time (12-24h), nanosheet-like particles of thickness 70-100 nm were obtained, which got self-assembled to form 3D architecture. Interestingly, it was noticed that after calcination at

Dalton Transactions Accepted Manuscript

300°C, the morphology of the corresponding samples remained the same. Figure 6 shows the FESEM images of the calcined samples prepared hydrothermally at 150°C for 2h (Fig. 6a, b) and 5h (Fig. 6c, d), which also revealed chrysanthemum-like architectures composing of self-assembled nanorods of Co_3O_4, whereas the FESEM microstructures of the calcined samples for 12h (Fig. 6e, f) and 24h (Fig. 6g, h) reaction times indicated self-assembly of nanosheet-like particles.

Figure 7A shows the TEM images of the calcined samples prepared hydrothermally at 150°C for (a) 2h, (b) 5h, (c) 12h and (d) 24h. It indicated the rod-like particles of Co_3O_4 for 2h and 5h reaction times, which were formed by the self-assembly of nanometer sized (5-20 nm) particles in 1D direction as observed by their higher magnification images (Fig. S2a,b, ESI). However, with increase in synthesis times up to 12h-24h, sheet-like structures were generated. Higher magnification images of TEM reveal that interparticle pores were developed for 2h and 5h reaction times (Fig. S2a,b, ESI), while for higher reaction times (12-24h), channel-like pores were formed (Fig. S2c,d ESI). Close inspection of the images for 12-24h prepared samples revealed that some channel pores became discontinued or blocked, which could account the restriction of desorbing condensed liquid generated by capillary condensation, resulting the lower pore volume instead of more increase in surface area compared to 2-5h prepared samples. It is clear that interparticle pores generated for 2-5h reaction time are larger in size than those in the channel-like pores for higher reaction times (12-24h). It was supported by the pore sizes determined by the BJH method. The selected area electron diffraction (SAED) patterns of Co_3O_4 indicated the polycrystalline nature of the particles (Fig. S3, ESI). The bright spots of the concentric rings matched well with the Co_3O_4 planes obtained from XRD. Figure 7B shows the HR-TEM of the calcined samples prepared for (a) 2h and (b) 5h indicating d-spacing of 0.28 nm which was attributed to the (220) lattice planes of cubic Co_3O_4 phase. For 5h reaction time, an additional d-spacing of 0.25 nm was

Dalton Transactions Accepted Manuscript

noticed which matched with (311) lattice plane. Interestingly, the d-spacing (0.47 nm) corresponding to the (111) lattice planes for 12h (Fig. 8c) and 24h (Fig. 8d) treated samples was due to nanosheet structure of Co_3O_4.[32]

A probable formation mechanism of Co_3O_4 with different morphologies in the presence of urea is illustrated in Scheme 1. Under hydrothermal reaction condition at 150°C, urea decomposes slowly with the formation of NH_3 and CO_2 followed by their hydrolysis producing CO_3^{2-} and OH^- ions. With the release of NH_3 accompanying with relatively low solubility of CO_2 in the aqueous solution via urea hydrolysis, the solution becomes alkaline.[33] It favours for heterogeneous nucleation of Co species. With the stepwise hydrolysis of urea, in the reaction medium, cobalt salt interacts with the anions (CO_3^{2-} and OH^-) forming the nuclei of cobalt hydroxy carbonate. The OH^- ions are adsorbed on Co^{2+} exposing facets, which enhance the polarity of negatively charged cobalt hydroxy carbonate. As a result, a dipolar interactions can occur leading to 3D self-assembly via electrostatic force and hydrogen bonding.[34] The reactions involved in the system are expressed as follows:

$$CO(NH_2)_2 + xH_2O \rightarrow 2NH_3 + CO_2 + (x-1)\ H_2O \quad (1)$$

$$NH_3 + H_2O \rightarrow NH_4^+ + OH^- \quad (2)$$

$$CO_2 + H_2O \rightarrow CO_3^{2-} + 2H^+ \quad (3)$$

$$Co^{2+} + xOH^- + 0.5\ CO_3^{2-} + 0.11H_2O \rightarrow Co(OH)_x(CO_3)_{0.5}.\ 0.11H_2O \quad (4)$$

$$2Co^{2+} + 2OH^- + CO_3^{2-} \rightarrow Co_2(OH)_2(CO_3) \quad (5)$$

$$6Co(OH)_x(CO_3)_{0.5}.\ 0.11H_2O \rightarrow 2Co_3O_4 + 3CO_2 + nH_2O\ (n = 3(x+0.22)) \quad (6)$$

$$3Co_2(OH)_2(CO_3) \rightarrow 2Co_3O_4 + 3CO_2 + 3H_2O \quad (7)$$

Dalton Transactions Accepted Manuscript

It is clear that urea plays an important role in the formation of rod or sheet-like particles. The formation of NH_3 and CO_2 from urea exists in the form of bubbles in aqueous solution.[35,36] These bubbles acts as soft templates. At the initial stage, the nanoparticles of hydrated cobalt hydroxy carbonate grow around the bubbles forming hierarchical structure in which the particles are loosely packed. By Ostwald ripening process, the particles grow along a certain crystallographic axis with the exposure of {110} plane forming 1D nanorods. With higher reaction time (12-24h), the nanorod-like particles stack together forming nanosheet-like particles.

To investigate the nanorod to nanosheet-like morphology, an intermediate synthesis time (8h) was chosen between 5h and 12h. Interestingly, it was observed that nanorod-like particles started stacking (Fig. S4a for as-prepared sample and Fig. S4b for calcined (300^{o}C) sample, ESI)) together, and the particles were tightly packed in the structure. It is understood that transformation of $Co(OH)_x(CO_3)_{0.5}.\ 0.11H_2O$ phase to $Co_2(OH)_2(CO_3)$ phase could also play a significant role for changing rod-like particles to sheet-like particles. After 5h, the adsorption of more negatively charged species (OH^- ions) on $Co_2(OH)_2(CO_3)$ particles enhances polarity.[34] As a result, more electrostatic interaction among $Co_2(OH)_2(CO_3)$ particles compared to that among $Co(OH)_x(CO_3)_{0.5}.\ 0.11H_2O$ species favoured sheet-like self-assembly in the former. For the as-prepared sample of 8h, a complete transformation of $Co_2(OH)_2(CO_3)$ phase occurred. It was identified by XRD (Fig. S5a, ESI) and FTIR (Fig. S6a, ESI) studies. After heating the sample at 300^{o}C, Co_3O_4 was formed as supported by XRD (Fig. S5b, ESI) and FTIR (Fig. S6b, ESI).

3.2 Catalytic study

Catalytic activity of the Co_3O_4 samples for the degradation of CSB in the presence of H_2O_2 was performed. As the degradation of CSB proceeded, the characteristic absorption of CSB at

Dalton Transactions Accepted Manuscript

λ_{max} = 618 nm gradually decreased. A blank (without using catalyst) experiment was performed for dye degradation in the presence of H_2O_2 to prove the catalytic performance of Co_3O_4. The trend of decrease in CSB degradation after catalytic reaction with time for different synthesis times followed as 5h>2h>12h>24h (Fig. S7, ESI). Figure 8A shows linear plot of $\ln(C_t/C_o)$ vs time, which confirmed pseudo-first order kinetics of the catalytic reactions. It is clear that dye concentration decreased with time, the rate of decrease of concentration for different synthesis times followed as 5h>2h>12h>24h having their rate constant values of $56.8x10^{-3}$ min^{-1}, $41.7x10^{-3}$ min^{-1}, $27.0x10^{-3}$ min^{-1}, and $9.1x10^{-3}$ min^{-1}, respectively. Figure 8B shows the degradation efficiency of the catalyst with time. It was noticed that the maximum degradation of 90%, 98%, 80% and 42% was obtained after 1h with the catalyst prepared at 150^oC for 2h, 5h, 12h and 24h, respectively. The stability of catalytic efficiency was checked for 4 cycles with the samples prepared for 5h reaction time (Fig. 8C). It shows that catalytic activity remained practically the same as the original sample indicating recyclable of the catalyst.

The mechanism for the catalytic decomposition of H_2O_2 in the presence of Co^{2+} and Co^{3+} in Co_3O_4 spinel is illustrated in scheme S1 (ESI). In this case the H_2O_2 is adsorbed on the catalytic surface producing hydroxyl ($OH^{\bullet}$) and peroxide ($HO_2^{\bullet}$) radicals.[37] These radicals react with Co^{3+} sites of catalytic surface. The free radicals also react with adsorbed H_2O_2. The reactions proceed via a chain process. Finally, the hydroxyl ($OH^{\bullet}$) radicals are formed. It is to be mentioned that H_2O_2 is adsorbed on the catalytic sites, which releases $OH^{\bullet}$ radicals in solution. In solution, these $OH^{\bullet}$ radicals degrade CSB.

From the above observation, it is clear that catalytic efficiency of Co_3O_4 was influenced by the different properties of the particles, namely, morphology and textural properties (surface area, pore volume and pore geometry). The particles with rod-like

Dalton Transactions Accepted Manuscript

morphology prepared for the reaction time of 2h and 5h had more catalytic active sites compared to those with sheet-like morphology synthesized for the reaction time of 12h and 24h. For the catalytic oxidation of CO, Xie *et al* proposed that Co_3O_4 nanorods preferentially exposed with {110} plane, favouring the presence of active Co^{3+} species at the surface.[38] As a result, the more catalytic active Co^{3+} sites prevail in nanorod morphology. In the present study, we also observed that Co_3O_4 nanorods with exposed {110} planes possess more catalytic active sites for the decomposition of CSB. The textural properties of the particles also played an important role for adsorption of CSB on catalytic suirface. With the same rod-like morphology, catalytic efficiency and rate constant were higher for the sample prepared for 5h synthesis time compared to those for the sample prepared for 2h synthesis time (Fig. S8, ESI). Due to higher BET surface area and pore volume of 5h-treated samples compared to 2h-treated sample, the adsorption of CSB on the catalytic surface was more for 5h synthesized sample, which facilitated the catalytic efficiency.[39] It is mentioned worthy that the increase order of BET surface area of the samples synthesized at different time periods are 2h<5h<12h<24h. However, the least catalytic efficiency and rate constant values resulted for the sample prepared for 24h followed by 12h. Therefore, it is interesting that not only BET surface area influenced the catalytic efficiency, but the pore geometry (pore shape and size) and pore volume were also important. By examining the pore geometry of the samples, it is clear that the abundance of interparticle mesoporosity and higher pore volume in rod-like structure (particles for 2h and 5h reaction time) were more accessible to catalytic reactions. However, with increase in synthesis time from 12h to 24h, the mesoporosity and pore diameter decreased resulting lesser catalytic activity. Some fraction of microporosity having lesser pore volume generated in sheet-like structure made a hindrance for catalytic reactions. The presence of larger pores in 2h and 5h-treated samples enhanced more adsorption as well as faster diffusion of CSB in mesoporous Co_3O_4, which facilitated the catalytic efficiency. On

Dalton Transactions Accepted Manuscript

the other hand, the smaller pores in 12h and 24h-treated sample retarded both the adsorption and diffusion of CSB in mesoporous Co_3O_4 resulting lesser catalytic efficiency. Therefore, it can be demonstrated that many factors like morphology, surface area, pore volume and pore geometry of the particles are important for catalytic reactions.

4. Conclusions

In summary, we have demonstrated a facile hydrothermal synthesis of Co_3O_4 nanostructures with controllable morphology and tunable textural properties via aqueous based route in the absence of templating agents. Catalytic performance for the degradation of Chicago Sky Blue 6B in the presence of H_2O_2 was studied with Co_3O_4 particles. The affects of morphology and textural properties on the catalytic behaviors of Co_3O_4 were examined. It was revealed that nanorod-like particles with higher pore volume and mesoporosity obtained from 2h and 5h treated samples were more active in catalysis compared to those of nanosheet-like particles obtained from 12h and 24h treated samples having smaller pore volume along with the presence of microporosity which made hindrance in catalytic activity. By tuning the crystal morphology and surface properties, Co_3O_4 and other transition metal oxides could be applicable in many other fields.

Acknowledgement

The authors would like to thank the Director of this institute for his kind permission to publish this paper. The authors (M. Roy and S. Ghosh) are thankful to CSIR for their fellowship. The Nano Structureed Materials Division is thankfully acknowledged for Raman spectra. The work was funded by DST-SERB Project, Government of India (No. GAP 0616).

References

Dalton Transactions Accepted Manuscript

1. W.Y. Li, L.-N. Xu and J. Chen, *Adv. Funct. Mater.*, 2005, **15**, 851.
2. P. Polzot, S. Laruelle, S. Grugeon, L. Dupont, J. M. Tarascon, *Nature*, 2000**, 407**, 496.
3. G. Wang, X. Shen, J. Horvat, B. Wang, H. Liu, D. Wexler, J. Yao, *J. Phys. Chem. C***,** 2009**, 113**, 4357.
4. M. Yada, Y. Inoue, M. Koikawa, T. Torikai, T. Watari, *CrystEngComm.*, 2012**, 14**, 7374.
5. T.-L. Lai, Y.-L. Lai, C.-C. Lee, Y.-Y. Shu, C.-B. Wang, *Catal. Today*, 2008**, 131**, 105.
6. H. Sun, H. Ming Ang, M. O. Tade and S. Wang, *J. Mater. Chem. A*, 2013, **1**, 14427.
7. X. Ke, J. Cao, M. Zheng, Y. Chen, J. Liu and G. Ji, *Mat. Lett.* 2007, **61**, 3901.
8. Y. Li, B. Tan, Y. Wu, *Nano Lett.,* 2008, **8**, 265.
9. X. W. Lou, D. Deng, J. Y. Lee, J. Feng, L. A. Archer, *Adv. Mater.*, 2008, **20**, 258.
10. Y. Wang, H. Xia, L. Lu, J. Lin, *ACS Nano*, 2010, **4**, 1425.
11. M. Wang, L. Zeng and Q. Chen, *Dalton Trans.*, 2011, **40**, 597.
12. L. Chen, J. Hu, R. Richards, S. Prikhodko, S. Kodambaka, *Nanoscale*, 2010, **2,** 1657.
13. X. Wang, H. Guan, S. Chen, H. Li, T. Zhai, D. Tang, Y. Bando, D. Golberg, *Chem. Commun.*, 2011, **47**, 12280.
14. K. Nakajima, T. Fukui, H. Kato, M. Kitano, J. N. Kondo, S. Hayashi, M. Hara, *Chem. Mater.*, 2010, **22**, 3332.
15. J. P. Cheng, X. B. Zhang, Y. Ye, J. P. Tu, F. Liu, X. Y. Tao, H. J. Geise, T. G. Van, *Microporous Mesoporous Mater.*, 2005, **81**, 73.
16. C.-A. Wang, S. Li, L. An, *Chem. Commun.*, 2013, **49**, 7427.
17. J. Rosen, G. S. Hutchings, F. Jiao, *J. Am. Chem. Soc.*, 2013, **135**, 4516.
18. Y. Xia, H. Dai, H. Jiang, L. Zhang, *Catal. Commun.*, 2010, **11**, 1171.

Dalton Transactions Accepted Manuscript

19. G. Wang, H. Liu, J. Horvat, B. Wang, S. Qiao, J. Park, H. Ahnidl, *Chem. - Eur. J.*, 2010, **16**, 11020.

20. J. Deng, L. Zhang, H. Dai, Y. Xia, H. Jiang, H. Zhang, H. He, *J. Phys. Chem. C*, 2010, **114**, 2694.

21. N. Dahal, I. A. Ibarra, S. M. Humphrey, *J. Mater. Chem.*, 2012, **22**, 12675.

22. Y. Li, B. Tan, Y. Wu, *J. Am. Chem. Soc.*, 2006, **128**, 14258.

23. N. Venugopal, D.-J. Lee, Y. J. Lee, Y.-K. Sun, *J. Mater. Chem. A*, 2013, **1**, 13164.

24. H. Wang, L. Zhang, X. Tan, C. M. B. Holt, B. Zahiri, B. C. Olsen, D. Mitlin, *J. Phys. Chem. C*, 2011, **115**, 17599.

25. J. Zheng, J. Liu, D. Lv, Q. Kuang, Z. Jiang, Z. Xie, R. Huang, L. Zheng, *J. Solid State Chem.*, 2010, **183**, 600.

26. A. K. Mohammed, K. T. McKenzie, *J. Environ. Sci.*, 2005, **17**, 869.

27. S.C. Petitto, E. M. Marsh, G. A. Carson, M. A. Langell, J. Mol. Catal. A: Chem., 2008, **1-2,** 49.

28. J. Yang, H. Cheng, R. L. Frost, *Spectrochim. Acta, Part A*, 2011, **78A**, 420.

29. R. Xu, H. C. Zeng, *J. Phys. Chem. B*, 2003, **107**, 12643.

30. H.-P. Cong, S.-H. Yu, *Cryst. Growth Des.*, 2009, **9**, 210.

31. C.W. Na, H.-S. Woo, H.-J. Kim, U. Jeong, J.-H. Chung and J.-H. Lee, *CrystEngCommn.,* 2012, **14**, 3337.

32. H. Liang, J. M. Raitano, L. Zhang and S.-W. Chan, *Chem. Commn.*, 2009, **48**, 7569.

33. J. H. Pan, X. Zhang, A. J. Du, H. Bai, J. Ng, D. Sun, *Phys. Chem. Chem. Phys.*, 2012, **14,** 7481.

34. J. H. Pan, Q. Huang, Z. Y. Koh, D. Neo, X. Z. Wang, Q. Wang, *ACS Appl. Mater. Interfaces*, 2013, **5,** 6292.

Dalton Transactions Accepted Manuscript

35. J. Sun, G. Chen, J. Wu, H. Dong, G. Xiong, *Appl. Catal. B: Environ.*, 2013, **132-133,** 304.

36. C. Zhou, Y. Zhao, T. Bian, L. Shang, H. Yu, L-Z. Wu, C-H. Tung, T. Zhang, *Chem. Commn.*, 2013, **49,** 9872.

37. S-S Lin, M. D. Gurol, Environ. Sci. Technol, 1998, **32,** 1417.

38. X. Xie, Y. Li, Z-Q. Liu, M. Haruta, W. Shen, *Nature*, 2009, **458,** 746.

39. C. Yu, X. Dong, L. Guo, J. Li, F. Qin, L. Zhang, J. Shi, D. Yan, J. Phys. Chem. C, 2008, **112,** 13378.

Dalton Transactions Accepted Manuscript

Figure Captions

Figure 1: XRD patterns of (A) as-prepared samples (B) calcined samples at different synthesis times: (a) 2h, (b) 5h, (c) 12h and (d) 24h; (•): orthorhombic hydrated cobalt hydroxy carbonate, (▲): monoclinic cobalt hydroxy carbonate.

Figure 2: FTIR spectra of (A) as-prepared samples and (B) calcined (300^{o}C) samples synthesized at 150^{o}C for (a) 2h, (b) 5h, (c) 12h and (d) 24h.

Figure 3: Raman spectra of the calcined (300^{o}C) samples synthesized at 150^{o}C for (a) 2h, (b) 5h, (c) 12h and (d) 24h.

Figure 4: (A) N_2 adsorption-desorption isotherms, and (B) pore size distributions of 300^{o}C calcined samples synthesized at 150^{o}C for (a) 2h, (b) 5h, (c) 12h and (d) 24h.

Figure 5: FESEM micrographs of the as-prepared samples prepared at 150^{o}C for (a) 2h, (b) 5h, (c) 12h and (d) 24h.

Figure 6: FESEM images of the calcined (300^{o}C) samples, shown in the order of increasing magnification at different hydrothermal times: (a), (b) for 2 h; (c), (d) for 5 h; (e), (f) for 12 h; and (g), (h) for 24 h.

Figure 7: (A) TEM images of the calcined (300^{o}C) samples obtained at 150^{o}C for (a) 2h, (b) 5h, (c) 12h and (d) 24h; (B) HRTEM images of the corresponding samples.

Figure 8: (A) Plot of $\ln(C_t/C_o)$ vs.time, (B) the degradation efficiency for the degradation of Chicago sky blue 6B (CSB) dye in presence of H_2O_2 without any catalyst (blank), and using Co_3O_4 catalyst prepared at 150^{o}C for (a) 2h (b) 5h (c) 12 h and (d) 24 h, and (C) rate constant values for the same degradation in four consecutive cycles using the same 5h treated samples.

Dalton Transactions Accepted Manuscript

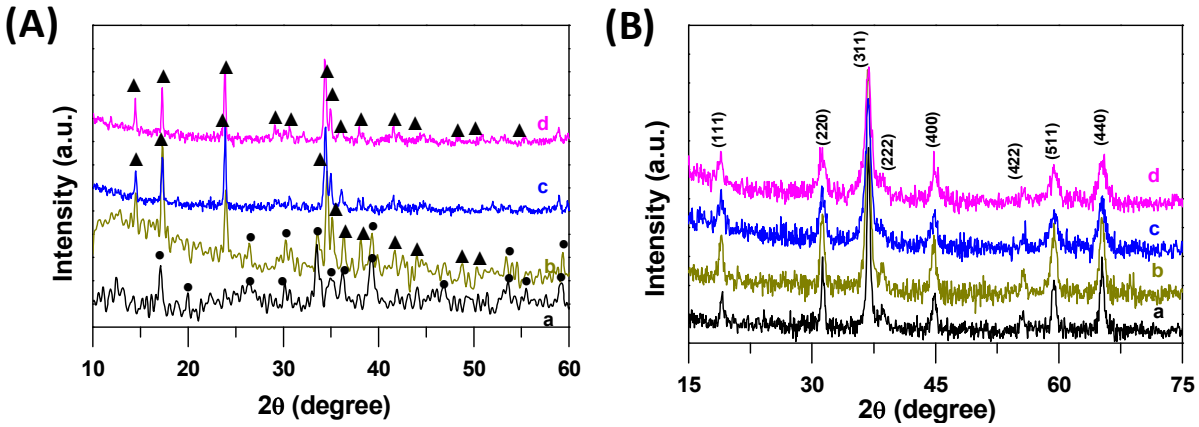

Figure 1: XRD patterns of (A) as-prepared samples (B) calcined samples at different synthesis times: (a) 2h, (b) 5h, (c) 12h and (d) 24h. (•): orthorhombic hydrated cobalt hydroxy carbonate, (▲): monoclinic cobalt hydroxy carbonate.

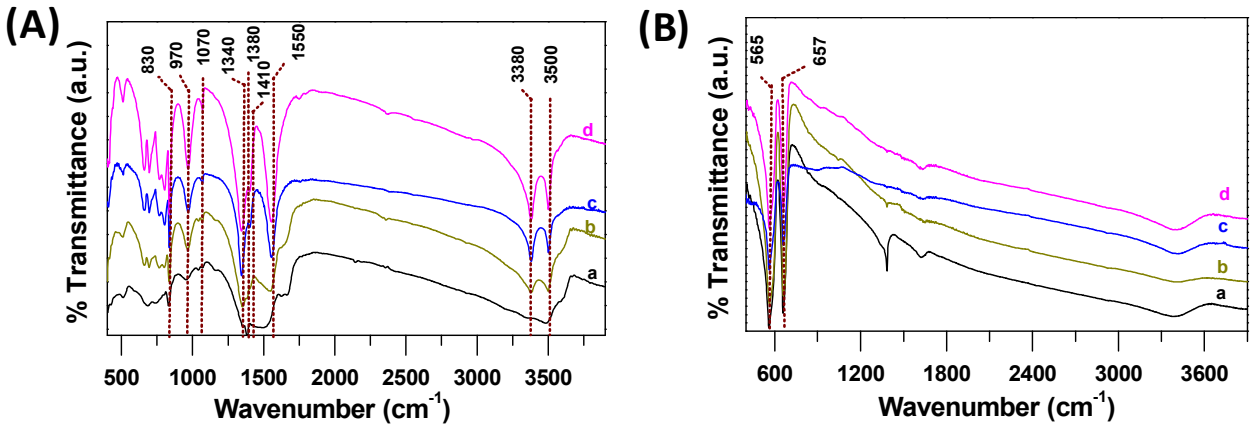

Figure 2: FTIR spectra of (A) as-prepared samples and (B) calcined (300°C) samples synthesized at 150°C for (a) 2h, (b) 5h, (c) 12h and (d) 24h.

Dalton Transactions Accepted Manuscript

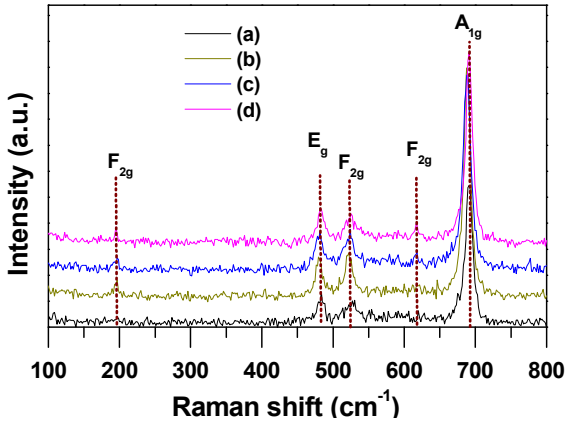

Figure 3: Raman spectra of the calcined (300°C) samples synthesized at 150°C for (a) 2h, (b) 5h, (c) 12h and (d) 24h.

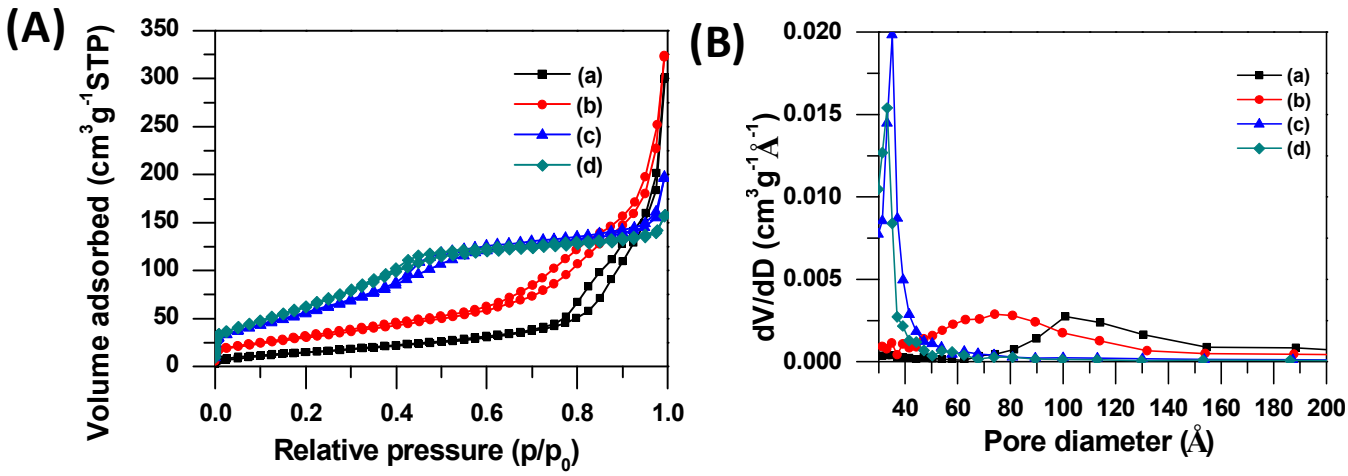

Figure 4: (A) N_2 adsorption-desorption isotherms, and (B) pore size distributions of 300°C calcined samples synthesized at 150°C for (a) 2h, (b) 5h, (c) 12h and (d) 24h.

Dalton Transactions Accepted Manuscript

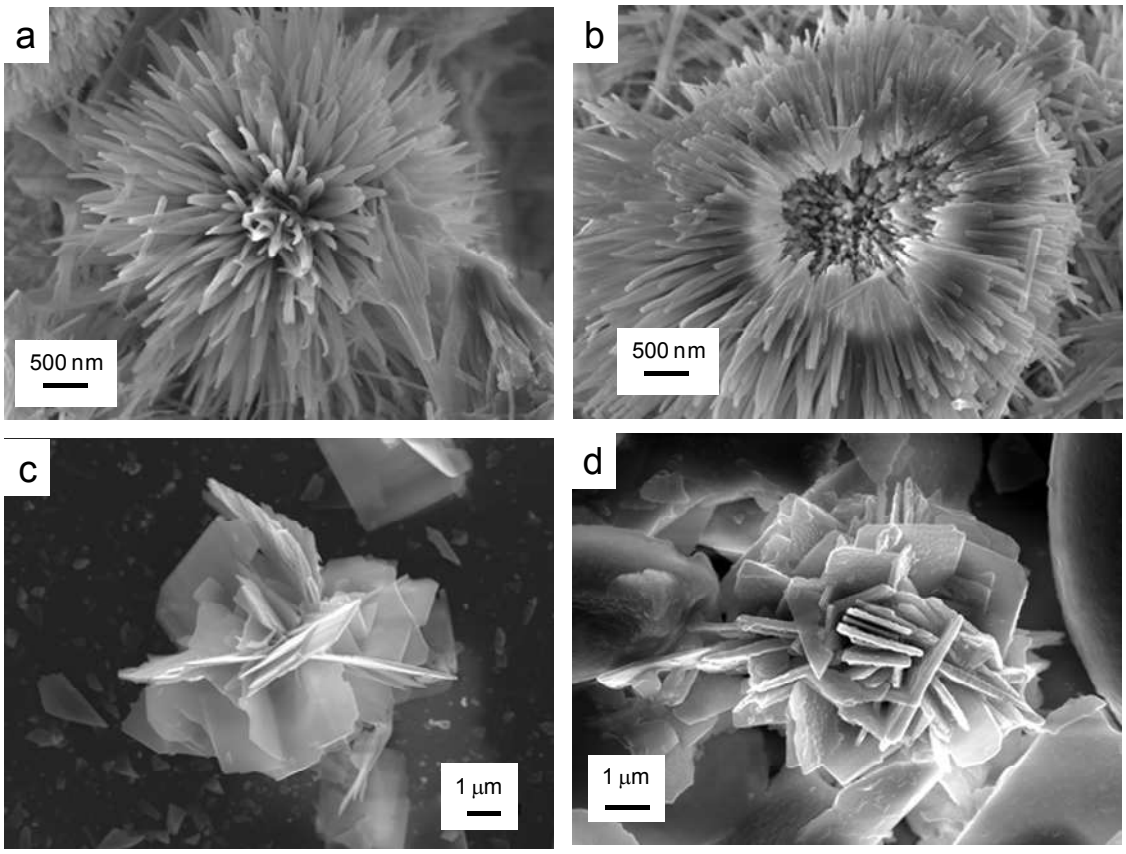

Figure 5: FESEM micrographs of the as-prepared samples prepared at 150°C for (a) 2h, (b) 5h, (c) 12h and (d) 24h.

Dalton Transactions Accepted Manuscript

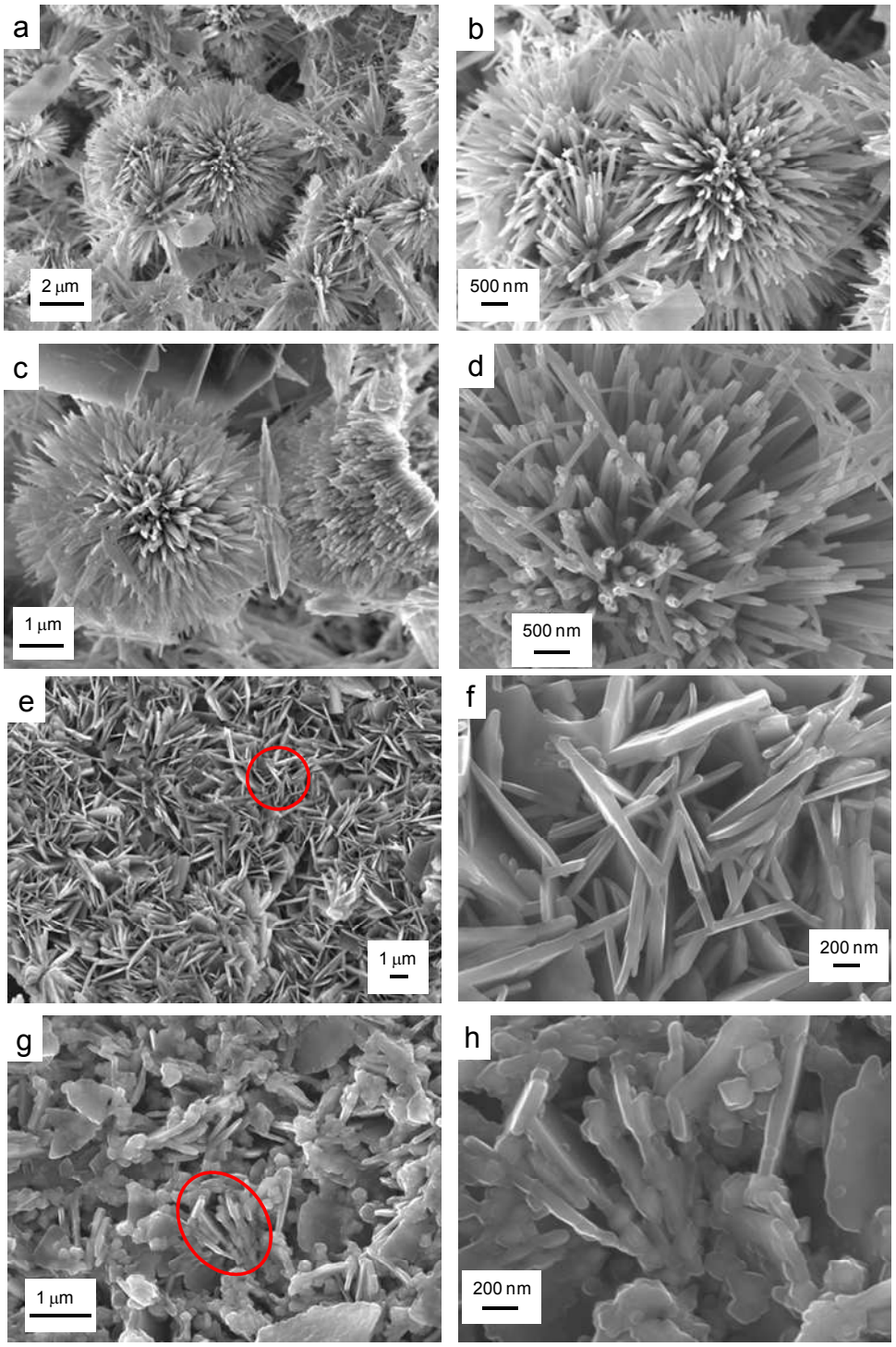

Figure 6: FESEM images of the calcined (300°C) samples, shown in the order of increasing magnification at different hydrothermal times: (a), (b) for 2 h; (c), (d) for 5 h; (e), (f) for 12 h; and (g), (h) for 24 h.

Dalton Transactions Accepted Manuscript

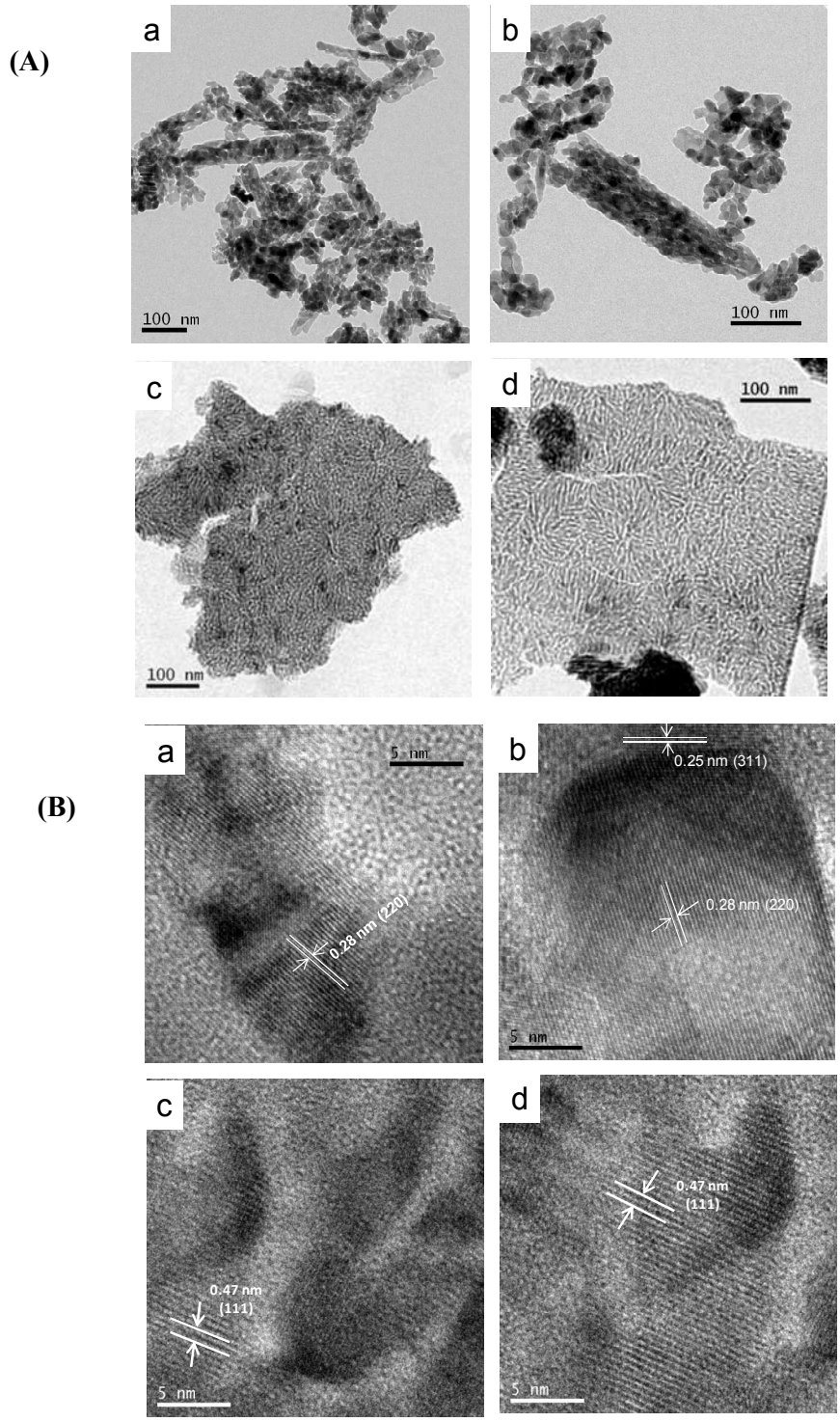

Figure 7: (A) TEM images of the calcined (300°C) samples obtained at 150°C for (a) 2h, (b) 5h, (c) 12h and (d) 24h; (B) HRTEM images of the corresponding samples.

Dalton Transactions Accepted Manuscript

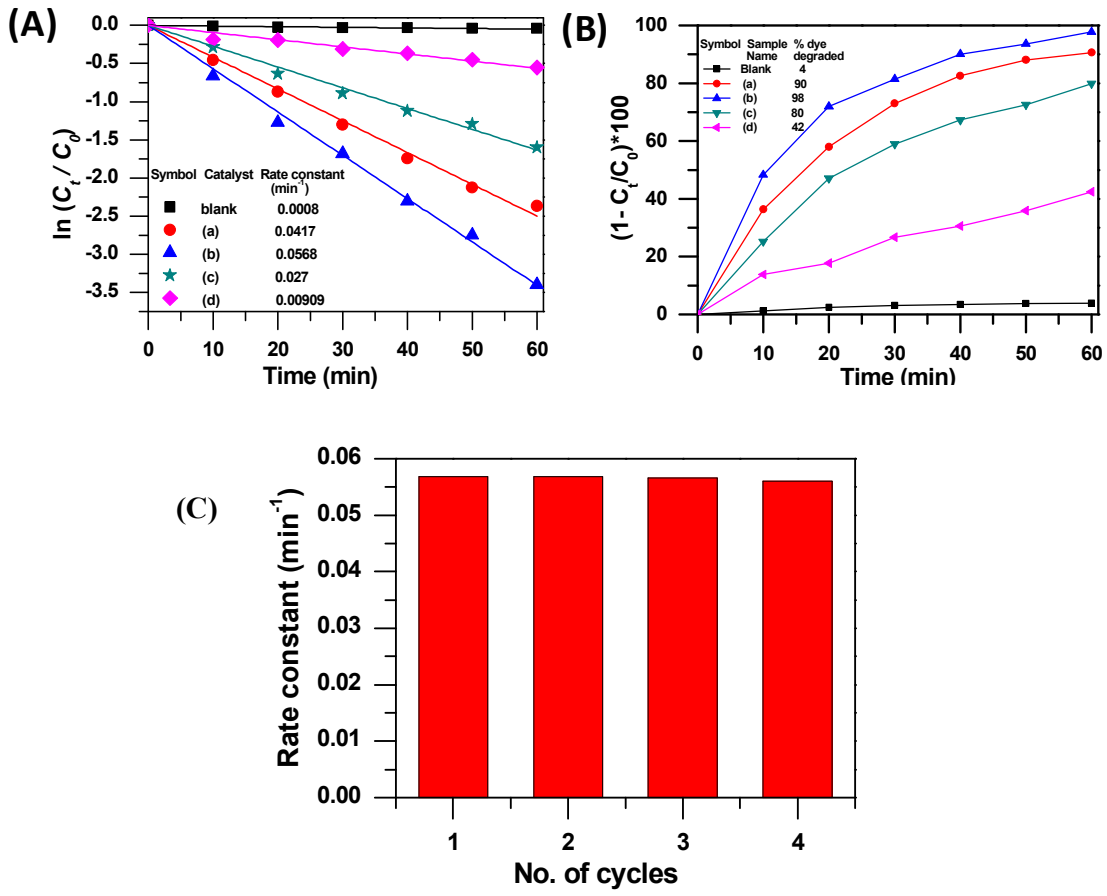

Figure 8: (A) Plot of ln*(C$_t$/C$_o$)* vs.time, (B) the degradation efficiency for the degradation of Chicago sky blue 6B (CSB) dye in presence of H_2O_2 without any catalyst (blank), and using Co_3O_4 catalyst prepared at 150^{o}C for (a) 2h (b) 5h (c) 12 h and (d) 24 h, and (C) rate constant values for the same decomposition in four consecutive cycles using the same 5h treated samples.

Dalton Transactions Accepted Manuscript

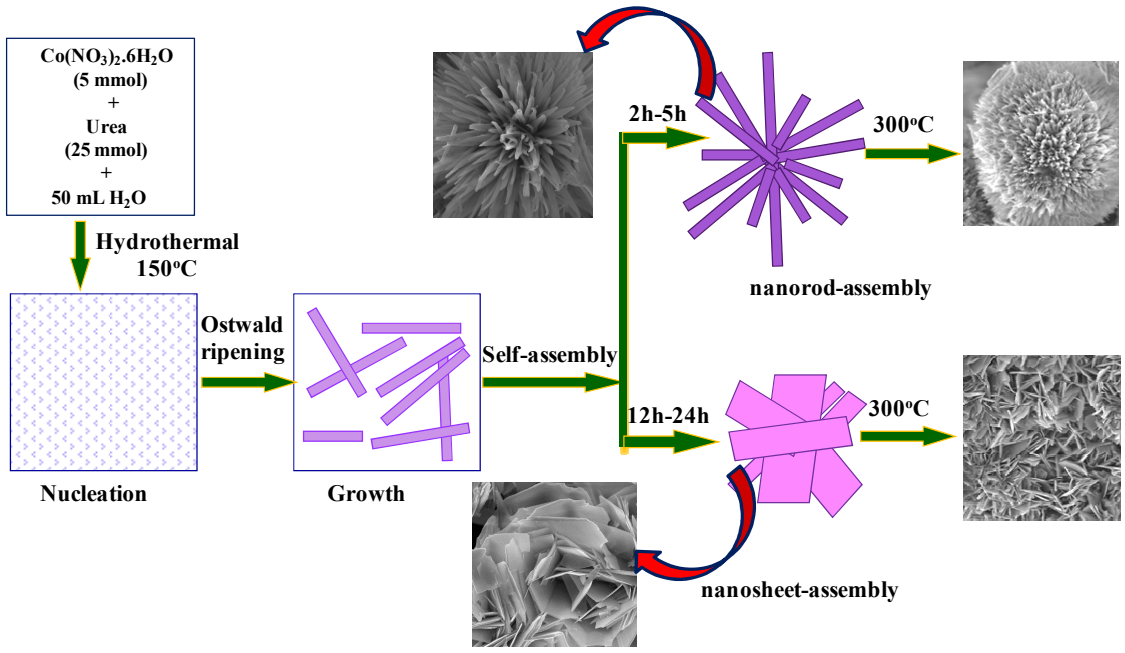

Scheme 1. Schematic representation of the proposed formation mechanism for shaped Co_3O_4.

Dalton Transactions Accepted Manuscript

Graphical Representation

Co_3O_4 nanostructure with controllable morphology and tunable textural properties synthesized via aqueous based route in the absence of templating agents were found to be an effective catalyst.

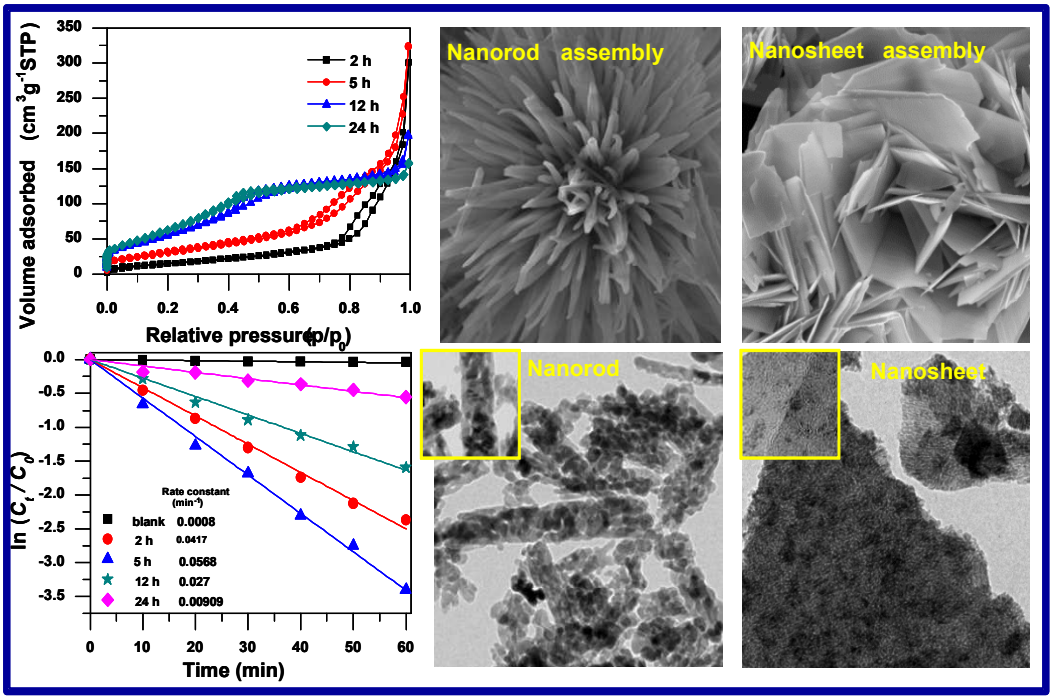

Dalton Transactions Accepted Manuscript